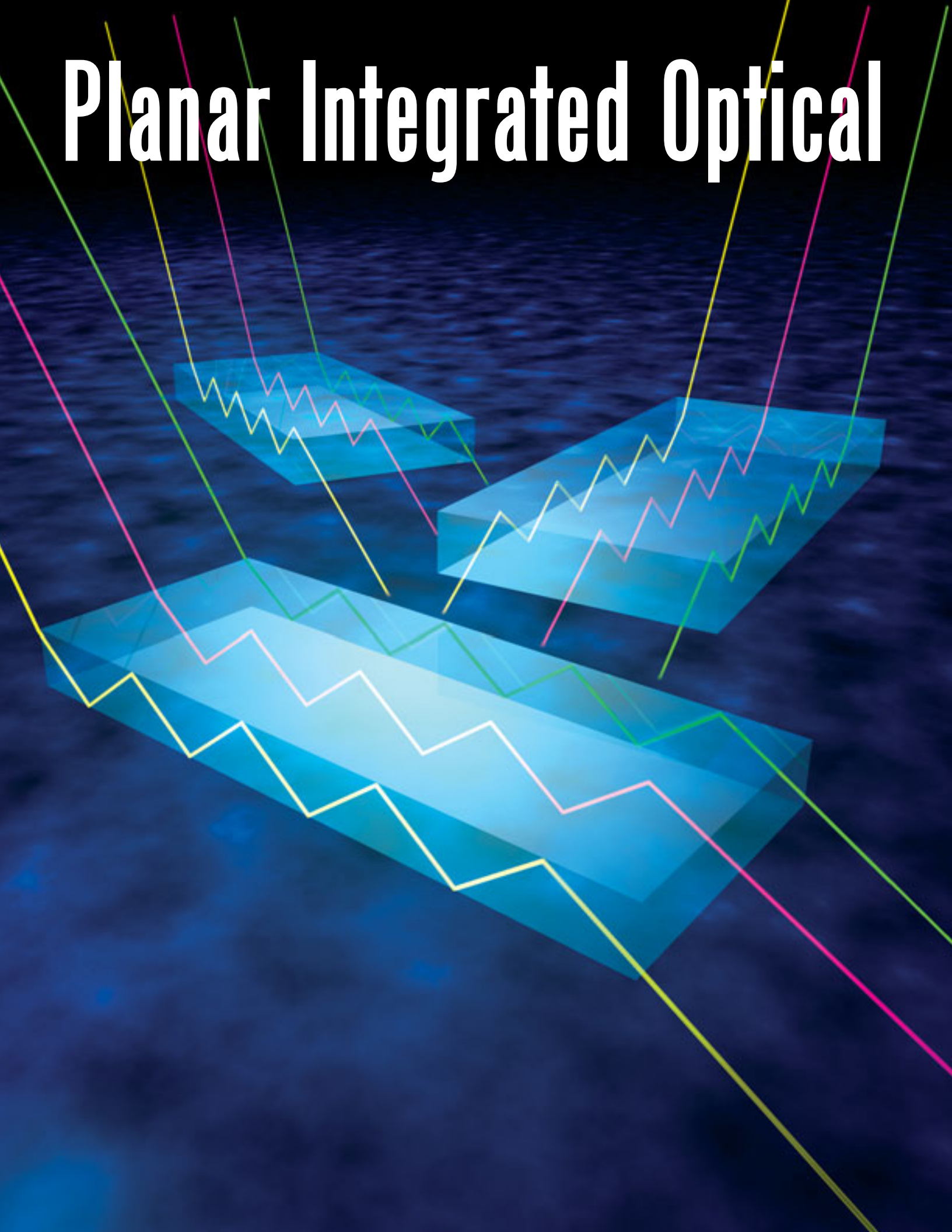


# Planar Integrated Optical



# Waveguide Spectroscopy

Improvements make it feasible to obtain  
absorbance spectra of thin films and  
submonolayers for thin-film characterization  
and chemical and biochemical sensing.

John Thomas Bradshaw  
Sergio B. Mendes  
S. Scott Saavedra  
University of Arizona

A

lthough the term “waveguide” may not be familiar to many people, applications of waveguiding technologies, such as fiber-optic-based communications, are widespread. Spectroscopists routinely use attenuated total reflection (ATR) to obtain FTIR spectra of thin films and the surfaces of bulk materials. The confinement of a light beam according to the principle of total internal reflection (TIR) occurs in both fiber-optic cables and internal reflection elements (IREs), which are used for data transmission and collecting IR spectral information, respectively. The cylindrical optical fiber and the planar IRE function as waveguides, a general term for structures that transport electromagnetic radiation via repeated TIR. Although waveguides can be created in numerous geometries, this article focuses on waveguides with a planar geometry that are used to study thin films and interfaces.

The fundamental work of Harrick and Fahrenfort is the basis for modern internal reflection spectroscopy (1, 2). They obtained IR-ATR spectra of absorbing materials brought into “optical contact” with an IR-transmitting IRE; this allows the evanescent field that extends just beyond the IRE surface to penetrate the sample. Because the penetration depth is comparable to the wavelength, the ATR spectrum is representative of the near-surface composition of the material. A large body of work followed shortly thereafter and provided the foundation for waveguide spectroscopy to develop into a distinct and still-evolving field (3, 4).

Most of the early experiments were performed with relatively thick IREs, typically >1 mm, which is much larger than the wavelength of the propagating light. In this type of device, the beam is totally reflected only a few times per centimeter of propagation along the length of the waveguide, and thus the beam interacts with the sample only a few times, or maybe only once. Consequently, the optical path length is relatively small, and low sensitivity results. However, because the number of reflections per centimeter is inversely proportional to IRE thickness, the path length can be greatly increased if a thinner waveguide is used (Figure 1; 5). A path length enhancement  $>10^3$  can be achieved by reducing the thickness of the waveguide to dimensions comparable to the wavelength of the propagating light. This type of structure, known as an integrated optical waveguide (IOW), supports the equivalent of  $10^3$ – $10^4$  reflections/cm of beam propagation and exhibits a proportionally larger path length relative to thick waveguide devices (6, 7).

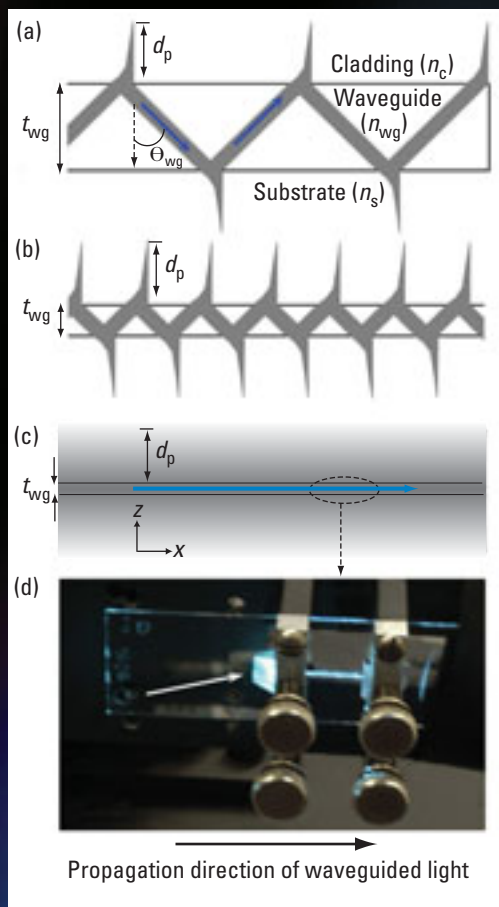


**FIGURE 1.** Waveguides basics.

A three-phase (media) planar waveguide is composed of the cladding material, the waveguiding layer, and the substrate material, with respective RIs  $n_c$ ,  $n_{wg}$ , and  $n_s$ , in which  $n_{wg} > n_s, n_c$ . The thickness of the waveguiding layer is  $t_{wg}$ ; the cladding and substrate are usually assumed to be infinitely thick. In a step-RI waveguide shown here,  $n_{wg}$  is constant across  $t_{wg}$ . (a) The guided light propagates along a zigzag path via repeated TIR. (b) As  $t_{wg}$  is decreased, the number of reflections per centimeter along the length of the waveguide (the  $x$  axis) increases. (c) In the IOW regime, when  $t_{wg} \approx \lambda$ , individual reflections are no longer physically discernible and the evanescent fields in the substrate and cladding are continuous along the  $x$  axis. (d) A guided mode entrapped in a single-mode, step-RI planar IOW, composed of a silica-titania sol-gel glass layer,  $\sim 300$ -nm thick, deposited on a soda lime glass microscope slide. A prism was used to couple the 488-nm output of an  $Ar^+$  laser into the waveguide. The white arrow shows the approximate path of the laser beam directed toward the prism hypotenuse.

The propagating electromagnetic radiation in a planar IOW and the evanescent field that penetrates into the adjacent cladding can be used to perform ATR, waveguide Raman (WRS), and waveguide fluorescence spectroscopies (WFS; 7). In ATR, the intensity of the guided light is attenuated because of the absorbing components present in the cladding. In WRS and WFS, the guided light is used as a source to excite Raman scattering or fluorescence emission of species in the IOW or cladding. Waveguide interferometry is the basis of a separate class of highly sensitive techniques in which the phase of the guided light is altered by changes in the physical structure of the IOW, such as adsorption

of a film of protein molecules to the waveguide surface (8, 9).

Major developments in planar IOW spectroscopy began in the 1980s (7, 8, 10, 11). Seminal work by Swalen, Rabolt, and others demonstrated the power of WRS for measuring the vibrational spectra of submicrometer-thick polymer thin films and monolayers of molecules adsorbed to waveguide surfaces (12). Further advances in waveguide design have made it feasible to acquire normal, unenhanced Raman spectra of submonolayer protein films (13). Notable applications of WFS include diffusion behavior of molecules in thin polymer films and IOW-based transducer platforms for biochemical and chemical sensing (14–17). Thick planar waveguides printed with arrays of bio-recognition molecules have been used for fluorescence detection of clinical analytes and toxic agents (18). IOW-based, UV-vis absorbance techniques, including IOW-ATR, have been applied to a wide variety of condensed-phase problems, such as monitoring molecular adsorption processes, measuring molecular orientation in immobilized protein films, and biochemical and chemical sensing (19–24). ATR configurations with thick planar waveguides have also been used to study various types of molecular films (25, 26).

A brief introduction is presented on the theory of waveguide spectroscopy, with an emphasis on ATR measurements. For more comprehensive information, such as waveguide fabrication, coupling, and other types of spectroscopy, other sources should be consulted (6, 7, 10, 27, 28).

## Fundamentals

Consider an interface between a waveguide and cladding with refractive indices (RIs) of  $n_{wg}$  and  $n_c$ , respectively ( $n_{wg} > n_c$ ). A light beam incident on this interface from the waveguide layer at an angle larger than the critical angle [ $\theta_{cr} = \sin^{-1}(n_c/n_{wg})$ , Snell's law] will have its optical power totally reflected, if both media are transparent. Repeated total reflection at the boundaries between a planar waveguiding layer and the adjacent media propagates the beam with minimal loss. The zigzag beam path in IREs represents a ray-optics model of light propagation (Figures 1a and 1b). When this path is projected along the guiding element, the beam propagation is described by an effective RI, given by  $N_{wg} = n_{wg} \sin \theta_{wg}$ , in which  $\theta_{wg}$  is the angle of TIR. This is a conceptual definition because a priori knowledge of  $\theta_{wg}$  is not possible; in practice,  $N_{wg}$  is determined by solving specific requirements. The beam is phase-shifted for each upward and downward traverse as well as upon reflection at the upper waveguide-cladding interface and the lower waveguide-substrate interface. For constructive interference to be achieved, the total phase shift during one "round-trip" should equal an integral multiple of  $2\pi$ . For those values of  $N_{wg}$  that satisfy this resonance condition, a propagating field (mode) along the waveguide is established (27, 29). The effective RI of all allowed modes must fall within the boundaries defined by the indices of the three layers, expressed as  $n_c, n_s < N_{wg} < n_{wg}$  ( $s$  for substrate), which applies to planar waveguides of any thickness. For a waveguide with a thickness  $t_{wg} \gg \lambda$  (e.g., visible light propagating in a 1-mm-thick glass microscope slide surrounded by air), thousands of modes are allowed at each wavelength. In contrast, only a few modes (or a single one) are allowed

in the IOW regime, where  $t_{\text{wg}} \approx \lambda$ . When  $t_{\text{wg}}$  is less than the “cutoff” thickness of the waveguide, usually a fraction of  $\lambda$ , no guided modes are supported.

Up to this point, we have considered beam propagation in a waveguide primarily from the perspective of ray optics, which provides an accurate description when  $t_{\text{wg}} \gg \lambda$ . However, the ray-optics model becomes increasingly approximate in the IOW regime. Here, the discrete reflections depicted schematically in Figures 1a and 1b overlap and become indistinguishable, as shown in Figure 1c. Figure 1d is a photograph of light propagating in a single-mode IOW with  $t_{\text{wg}} \approx 350$  nm; for this waveguide, the ray-optics model predicts several thousand reflections per centimeter. Although the ray-optics model is still a useful approximation of waveguide performance in the IOW regime (30), an exact description requires a much more rigorous approach known as the full-wave model, which is based on a solution to Maxwell's equations (27). The full-wave model allows calculation of electric field amplitudes across IOW structures by the development of relationships between the electric and magnetic field components of the propagating light.

Although the power of a light beam undergoing TIR is totally reflected back into the incident medium, solution of Maxwell's equations shows that an electromagnetic field will also be present in the lower-RI media (both cladding and substrate) surrounding the waveguide. Thus, some of the electromagnetic energy of the propagating beam is stored in the cladding and substrate. This evanescent field decays exponentially with distance from the waveguide surface; the distance at which it decreases to  $1/e$  of its value at the interface is the penetration depth,  $d_p$ , which is typically a fraction of  $\lambda$  and is given by

$$d_p(c,s) = \frac{\lambda}{2\pi(N_{\text{wg}}^2 - n_{c,s}^2)^{1/2}}$$

in which  $c$  and  $s$  refer to the cladding and substrate, respectively. The evanescent field is therefore localized near the waveguide-cladding and waveguide-substrate interfaces; at distances a few times  $d_p$ , the field strength is negligible.

Typically, only the volume penetrated by the evanescent field on one side of the waveguide, usually the upper cladding side, is used to perform waveguide spectroscopy. Changes in the optical properties of the material(s) occupying the evanescent volume of the cladding can be detected as changes in the power or the phase (usually both) of the propagating beam. For example, the introduction of light-absorbing molecules into the evanescent volume

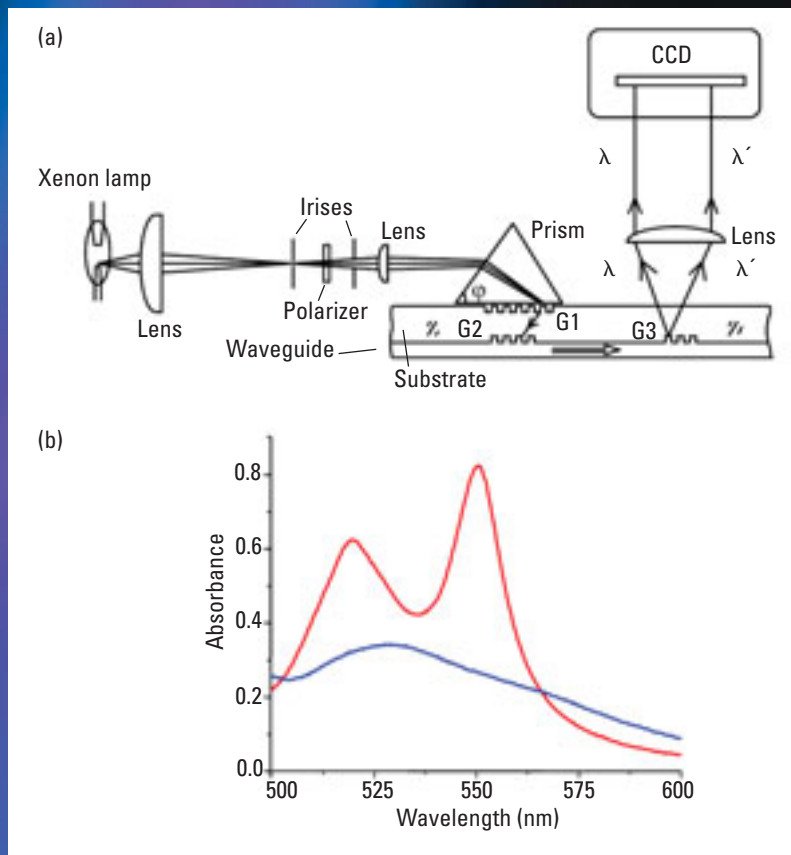


**FIGURE 2.** First-generation broadband IOW-ATR spectrometer.

(a) Light from a xenon lamp was spatially filtered and focused onto the achromatic incoupler, which consisted of a prism (base angle  $\phi$ ) and two gratings (G1 and G2). (b) Spectra of an adsorbed cytochrome *c* film measured with the IOW-ATR instrument in (a). Spectra were collected after the protein film was reduced with dithionite (ferrocyanochrome *c*, red line) and again after it was oxidized with ferricyanide (ferricytochrome *c*, blue line). (Adapted from Ref. 34.)

alters the imaginary part of the RI of the evanescent volume, and this change can be detected as attenuation of the power of the propagating beam—this is the basis of IOW-ATR spectroscopy (30). The introduction of material(s) with a real part of the RI different than that of the cladding material can be detected as a change in the phase of the propagating beam—this is the basis of waveguide interferometry (8, 9).

If the electric field intensity distribution provided by the full-wave model is known, then the evanescent optical path length in an IOW-based spectroscopic experiment can be calculated exactly. However, when analyte molecules introduced into the evanescent volume cause only a small perturbation in the electric field distribution of the mode, the ray-optics model is sufficiently accurate (30). For a monolayer of molecules supported on a single-mode planar IOW that has a step-RI profile (i.e.,  $n_{\text{wg}}$  is constant across  $t_{\text{wg}}$ ), both models predict that the tightly con-

finer field provides a path length enhancement of  $10^3$ – $10^4$  relative to either single-pass transmission geometry or single-reflection ATR geometry.

This sensitivity enhancement also theoretically applies to ATR measurements performed using a single-mode optical fiber. However, the power that can be coupled into a single-mode fiber from a typical broadband light source is very limited; only one mode in each polarization is allowed because of both lateral and transverse confinement. If a thermal source (3000 K, emissivity = 0.33, vis-

chemical sensing (19–22, 24). However, measuring a broadband ATR spectrum potentially offers considerably more information about the physicochemical properties of the sample and thus was recognized early on as a technologically useful enhancement (33). Numerous attempts to address the spectral bandwidth problem have been reported but had limited success (29). Mendes reported the first truly successful solutions when he tested two different approaches for achieving achromatic coupling into a single-mode, planar IOW (29, 34, 35).



**Notable applications of waveguide fluorescence include diffusion behavior of molecules in thin polymer films and IOW-based transducer platforms for biochemical and chemical sensing.**

ible) is used, the coupled power is theoretically limited to  $\sim 0.02$  nW/nm for each polarization (31, 32). Such low powers are problematic for absorbance measurements, which typically rely on a few decades of power attenuation for dynamic range.

In contrast, a planar waveguide only confines light in the transverse direction (i.e., normal to the waveguide plane) and thus supports more modes, typically 100–1000, in the lateral dimension. All of these modes can potentially be excited by a broadband light source. Coupling a 100–1000-fold higher power into the waveguide simplifies signal detection. Thus, performing ATR spectroscopy using single-mode planar waveguide geometry is equivalent to performing hundreds of similar measurements in parallel with single-mode optical fibers.

The major methods used to launch light into the bound mode(s) of an IOW are prism, grating, endfire, and taper coupling (7, 28). Because prism and grating coupling provide better control over mode selection and polarization than endfire or taper coupling, they are used more frequently for IOW-based spectroscopy. Regardless of the method used, the effective RI of the light propagating in the coupling element must match  $n_{wg}$  of the mode for light to be launched into the waveguide.

### Broadband IOW-ATR spectroscopy

Although the single-mode IOW platform is significantly more sensitive than thicker IREs, it does present some significant technical challenges. A major one is the typically narrow spectral bandwidth of operation. For a single-mode IOW, each wavelength of a particular mode propagates (from a ray-optics perspective) at a unique  $\theta_{wg}$ , which in turn corresponds to a unique incoupling angle for a beam impinging on a prism or grating coupler (6, 7, 27). Therefore, for a broadband light beam to be launched into a single-mode IOW, each wavelength must be incident at its corresponding “correct” angle to yield a propagating mode.

Because achieving this condition is technically difficult, almost all IOW-ATR measurements reported have been performed over a very narrow spectral bandwidth. Monochromatic IOW-ATR spectroscopy has been used extensively for surface analysis and

The first-generation broadband IOW-ATR spectrometer (Figure 2a) contained a novel multicomponent incoupler made of a prism and two gratings. It dispersed a  $\sim 100$ -nm-width band of visible light from a xenon arc lamp at the corresponding propagation angles appropriate for each wavelength constituent, yielding a spectrum of bound waveguide modes (29, 34). After propagating for up to several centimeters, the light was outcoupled and dispersed by a third diffraction grating onto a CCD array detector. Broadband operation was achieved because the incoupler matched the chromatic dispersion of the step-RI IOW, a 400-nm Corning 7059 glass layer deposited on a fused silica substrate. In the design phase, several physical parameters of the incoupler (e.g., grating periods, prism material, incident angle) were iteratively optimized to “match” the IOW to achieve achromatic incoupling. Broadband IOW-ATR spectra were obtained of a hydrated submonolayer of a protein, horse-heart cytochrome *c*, adsorbed to the 7059 glass waveguide surface (Figure 2b). These spectra clearly demonstrate the unprecedented combination of spectral bandwidth and path length enhancement ( $>1000$  relative to a transmission geometry) provided by this spectrometer.

A much simpler design was the basis of a second-generation spectrometer with a 110-nm spectral bandwidth (35). In this case, a commercially available glass material with optical parameters that matched the 7059 IOW structure was used to fabricate a prism incoupler. This single-component incoupler was technically much simpler to fabricate than the prism/dual-grating incoupler used in the first-generation spectrometer and required less precise alignment to achieve achromatic coupling.

The broadband coupling approaches developed by Mendes and co-workers demonstrated the technical feasibility of multichannel planar IOW-ATR spectroscopy over a 100-nm bandwidth. However, practical disadvantages have hampered implementation of both approaches. First, both the single-prism and multicomponent incouplers required custom fabrication to match a particular IOW. Thus, if the structure of the IOW was altered (e.g., the composition of the waveguiding layer was changed), then a different incoupler would be required. Second, the optical prop-

agation loss (primarily due to scattering) of the sputtered 7059 glass IOWs is 1 dB/cm. This value is acceptable for ATR measurements. However, 7059 glass IOWs are readily etched when they are cleaned with strong oxidizing solutions; this greatly increases propagation loss.

Bradshaw et al. recently described a third-generation IOW-ATR spectrometer that uses a technically simpler approach to broadband coupling than its achromatic predecessors and can be applied to a broader range of IOWs (36). In this case, the IOW was a sol-gel derived, silica-titania glass layer, 300–400-nm thick, deposited on soda lime glass. The propagation loss of this type of waveguide is ~0.2 dB/cm, which is ~5× less than that of a 7059 IOW (37). Furthermore, the surface of the silica-titania glass IOW can be repeatedly cleaned in strong acids without significant degradation.

However, the most significant departure from the work of Mendes et al. was that the incoupling method was not achromatic. An incident light beam was focused on the prism incoupler (Figure 3a) with a numerical aperture (NA) sufficiently large to ensure that all wavelengths were incident at all angles that launched a propagating mode. Thus, for each wavelength a small fraction of the incident light was coupled into the IOW over a small angular range centered at the corresponding correct incoupling angle; outside this range, the incident light was rejected. Kato et al. used an IOW-ATR spectrometer constructed around a planar IOW with a gradient-RI profile to demonstrate the potential of the large-NA approach (38). They used an optical fiber to direct light to the incoupling prism, a second fiber to collect light from the outcoupling prism, and a scanning monochromator for single-channel spectral acquisition.

Success in implementing the large-NA approach depends on the amount of light per nanometer coupled into the waveguide versus the amount rejected by “incorrect” angular incidence. Figure 3b shows white light being guided and then dispersed at an outcoupling grating; the spectral bandwidth of the outcoupled light is clearly visible on a sheet of paper placed a few centimeters from the grating.

The spectra in Figure 3c illustrate the significant improvement in bandwidth and performance of the third-generation spectrometer relative to the older first- and second-generation instruments (36). In those cases, achromatic incoupling was unsuccessful at wavelengths <500 nm because of the “steep” dispersion of a 7059 glass IOW in this region of the spectrum (29, 34, 35). In contrast, incoupling white light with the large-NA approach extends the bandwidth

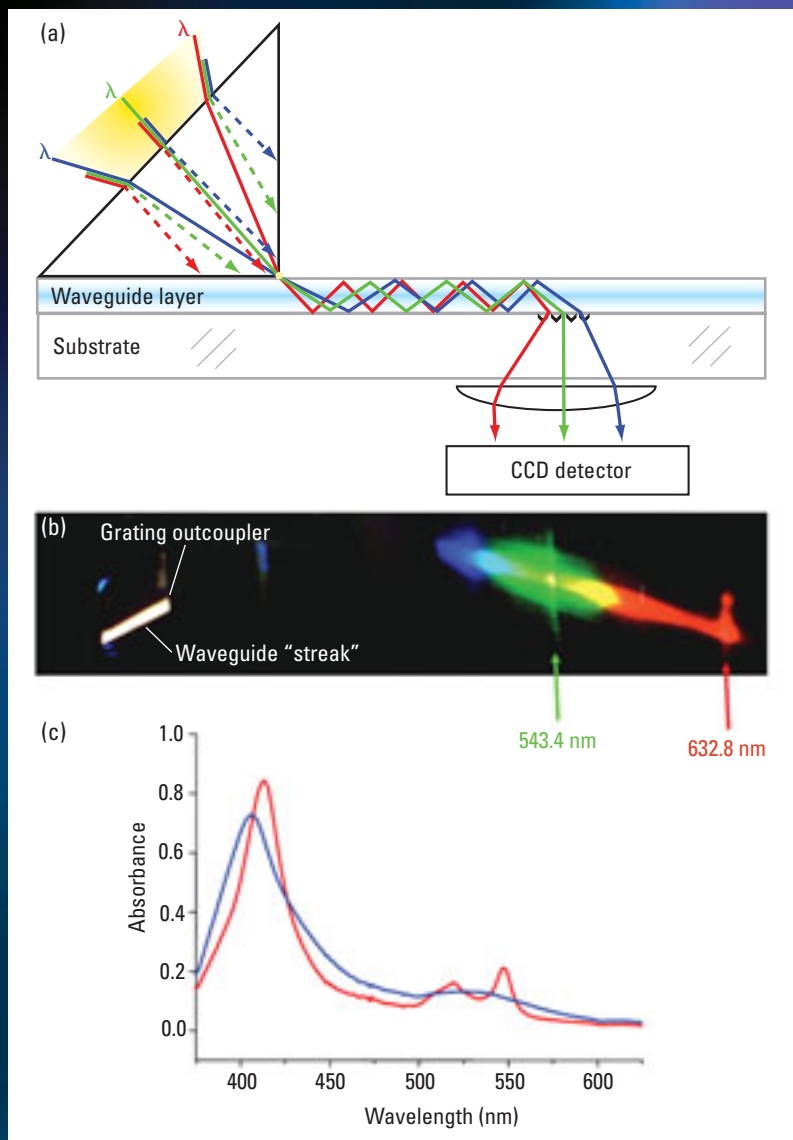


**FIGURE 3.** The large-NA approach.

For each wavelength component (colored  $\lambda$ ), a fraction of the incident light is coupled into the waveguide. (b) A commercially available SF6 glass prism was used as the incoupler to launch light from a xenon lamp into the same type of planar IOW shown in Figure 1d. Two helium-neon lasers emitting at 543.4 and 632.8 nm were collinearly aligned with the xenon lamp and launched simultaneously into the waveguide. Scattering from the spectrum of propagating modes produces the white streak on the left. Black paint was applied to the underside of the substrate to “strip” modes propagating in the substrate; consequently, the streak arises only from modes propagating in the waveguide layer. The streak disappears when the guided light encounters the diffraction grating, at which the light is outcoupled and dispersed. The spectral bandwidth of the outcoupled light is visible on a sheet of paper placed a few centimeters from the grating. Blocking the xenon source produces an outcoupled spectrum (not shown) containing only 543.4 and 632.8 nm light; the positions of these lines are used for wavelength and position calibration. (c) Spectra of a submonolayer of chemically oxidized (blue) and chemically reduced (red) cytochrome *c* adsorbed to a sol-gel glass waveguide surface measured with the IOW-ATR instrument in (a).

down to at least 390 nm; the total bandwidth exceeds 200 nm, twice that of the spectrometers based on achromatic coupling. The coupling efficiency in the large-NA approach is inherently low because only a small spectral width is coupled into the IOW for each angle. Much of the remainder is directed into radiation and substrate modes; this may pose a significant problem if

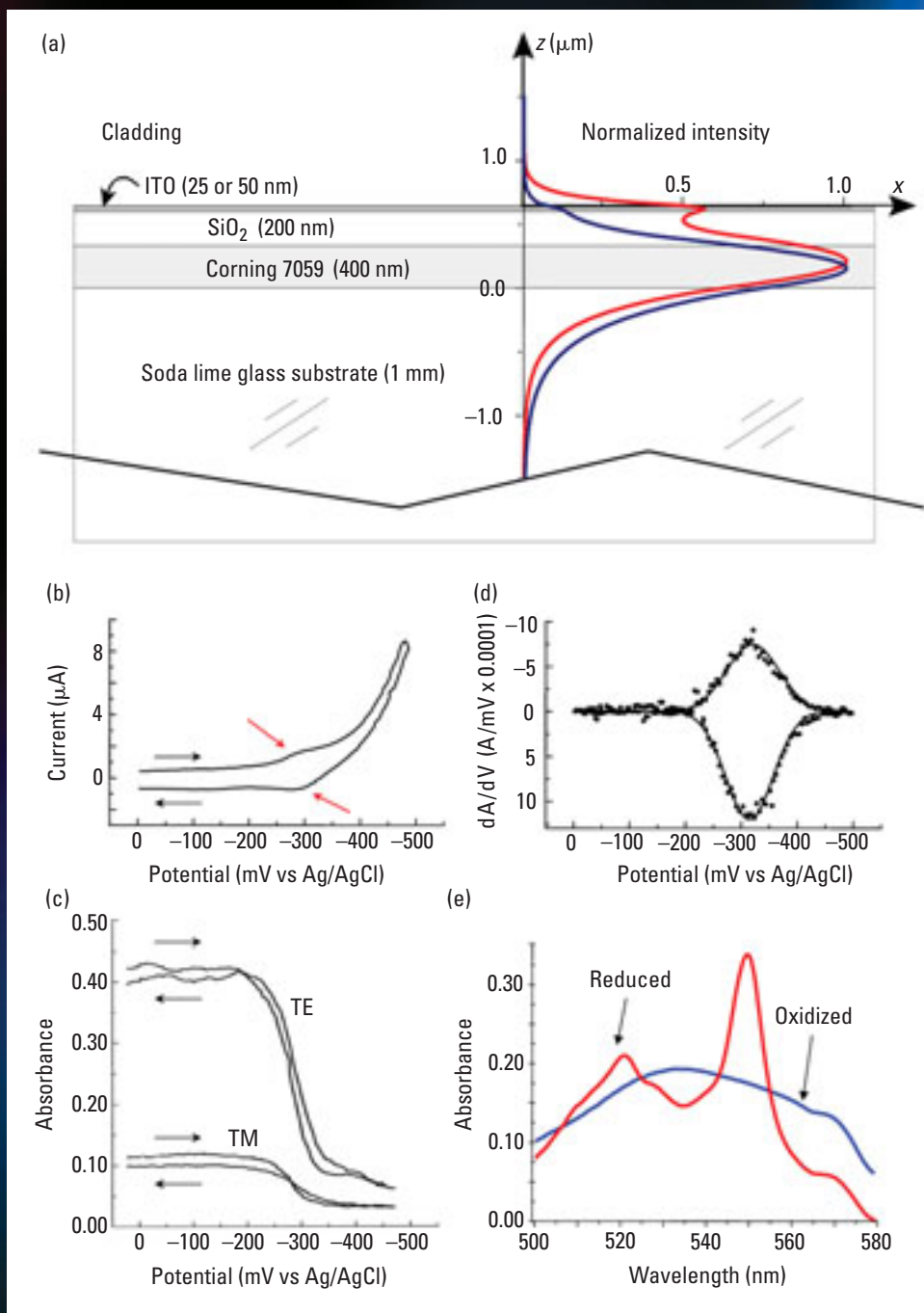


**FIGURE 4.** Single-mode EA-IOW-ATR spectroscopy.

(a) Schematic of the EA-IOW structure. A pair of diffraction gratings (not shown) was fabricated in the substrate prior to deposition of the Corning 7059/SiO<sub>2</sub>/ITO layers and was used to couple light into and out of the waveguide. The normalized electric field intensities along the *z* axis, calculated using the full wave model for an EA-IOW with a 50-nm ITO layer, are plotted for TE (red) and TM modes (blue). The evanescent field that extends into the cladding is used to perform ATR of molecular films at the ITO-cladding interface as a function of the potential applied to the ITO (working) electrode. (b) Conventional CV of a monolayer film of MB adsorbed to the EA-IOW, which was used as the working electrode. The black arrows indicate the direction of the scan; the red arrows indicate the region of scan in which faradaic current is observed. (c) Absorbance measured at 633 nm in TE and TM modes during CV of adsorbed MB. The experimental conditions are identical to those in (b). (d) Optical CV of adsorbed MB, reconstructed by taking the derivative of absorbance measured as a function of potential. The absorbance was measured in TM mode at 633 nm under experimental conditions identical to those in (b). (e) ATR spectra of a submonolayer of ferricytochrome *c* adsorbed to the EA-IOW from a neutral buffer. Broadband light was coupled into the TM mode using the large-NA method and outcoupled with a diffraction grating. A spectrum was collected after the cytochrome *c* film was electrochemically reduced (red) and then again after the film was electrochemically oxidized (blue). (Adapted with permission from Ref. 48.)

measures are not implemented to eliminate stray light before it reaches the detector. The achromatic approach can be used to reduce the angular width needed for broadband coupling, thereby improving coupling efficiency, but it may not be technically feasible to create an achromatic solution for all IOW structures. A combination of both approaches, particularly if the single-prism coupler is used (35), can potentially enhance the coupled bandwidth and minimize any stray-light problems.

### IOW-ATR spectro-electrochemistry

Combining spectroscopy and electrochemistry to study molecular films at electrode surfaces offers several major advantages (39, 40). Background from non-faradaic processes is largely eliminated; thus, detecting faradaic electrochemical processes is possible under conditions that would be problematic with conventional cyclic voltammetry (CV) techniques. In addition, the spectral response provides information that is complementary to that obtained from the conventional current or voltage response, such as the structure of the molecular film. However, transmission spectroelectrochemistry, in which the light path is perpendicular to the optically transparent electrode, may lack sufficient sensitivity to probe thin films of redox-active chromophores because of the inherently small optical path length (39, 40).

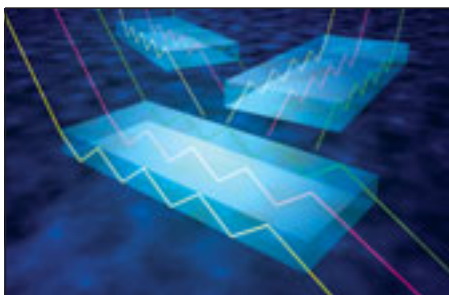
The significant advantages of performing spectroelectrochemistry with an ATR geometry were established in the 1960s (41–43). The evanescent field allows optical changes at the electrode-solution interface to be probed selectively without interference from the bulk so-

lution. In addition, a multiple-reflection arrangement can provide a substantial enhancement in sensitivity. For example, using a SnO<sub>2</sub>-coated/glass IRE that supported 5 reflections, Winograd and Kuwana observed a ~7-fold increase in sensitivity relative to a single-pass transmission experiment (41).

Itoh and Fujishima were the first to demonstrate the advantages of performing ATR spectroelectrochemistry in the IOW regime (44, 45). They fabricated IOWs that had a gradient-RI profile and were coated with an electroactive antimony-doped SnO<sub>2</sub> layer. For adsorbed films of methylene blue (MB), sensitivity enhancements ranging from 20 to 150 were seen, depending on the waveguide mode measured. Other research groups created similar multilayer, gradient-index, electroactive IOW (EA-IOW) structures, although in these cases the electroactive layer was composed of indium–tin oxide (ITO; 22, 46). Overcoating the ITO layer with another chemically selective layer created sensors for chlorine and ferricyanide.

The electric field intensity distribution in an IOW with a step-RI profile is more tightly confined than in an IOW with a gradient-RI profile; thus, the step-RI IOW is inherently more sensitive. To maximize the sensitivity of spectroelectrochemical ATR, Dunphy et al. created a single-mode, EA-IOW with a step-RI profile (47). The multilayer structure of this device is shown in Figure 4a, along with electric field intensity distributions calculated for transverse electric polarized light (TE) and transverse magnetic polarized light (TM) modes. The sensitivity of the step-RI EA-IOW to redox-induced absorbance changes in surface-confined films is at least 10<sup>4</sup>× greater than that obtained in a transmission geometry, far surpassing any previous spectroelectrochemical waveguide ATR device. This level of sensitivity makes it possible to explore the redox chemistries of submonolayer molecular films, including films of cytochrome *c*, MB, and rod-like molecular assemblies containing phthalocyanines (47, 48). Examples of data obtained on a film of MB with a surface coverage of 4% of a close-packed monolayer are shown in Figure 4, which illustrates some key features of EA-IOW-ATR spectroelectrochemistry.

The spectroscopic data are complementary to those obtained with conventional CV measurements. For example, in Figure 4c, the variation between the TE and TM signals arises from two sources: a difference in the optical path lengths of these modes and an anisotropic distribution of absorbance transition dipoles in the MB film. Thus, EA-IOW-ATR provides information about molecular orientation in films of redox-active chromophores. A comparison of Figures 4b and 4d clearly shows that the significant contribution from nonfaradaic background that interferes with



**Planar geometry offers better control over mode selection and polarization, and it is more compatible with organic and inorganic thin-film deposition technologies, most of which were designed for planar substrates.**

CV measurements is eliminated when optical detection is used; this makes it possible to probe electrochemical phenomena in very thin molecular films.

The first version of the step-RI single-mode EA-IOW was a monochromatic device. Matsuda, Doherty, and co-workers demonstrated the enhanced spectral information content provided by broadband ATR spectroelectrochemistry, although these groups used considerably less sensitive electroactive waveguide devices (IREs coated with ITO) to study thin films of redox-active dyes (49, 50).

Bradshaw et al. used the large-NA approach implemented for sol-gel IOWs (Figure 3a) to create a broadband EA-IOW spectrometer that combined the multidimensional information content of broadband ATR spectroelectrochemistry with the inherent sensitivity of the step-RI single-mode planar waveguide geometry (51). The spectrometer throughput was minimal at wavelengths <500 nm because of the limited trans-

mission of the ITO electrode layer in this spectral region; however, the bandwidth still exceeded 200 nm (i.e., from 500 to 700 nm). The optical performance of the spectrometer is demonstrated in Figure 4e. About 30% of a monolayer of ferricytochrome *c* was adsorbed to the ITO surface, and spectra were acquired after direct electrochemical reduction followed by direct oxidation. The combination of the newly developed broadband and ultrasensitive spectroelectrochemical capabilities demonstrates a powerful tool for studying the structural and electrochemical properties of thin, redox-active chromophores.

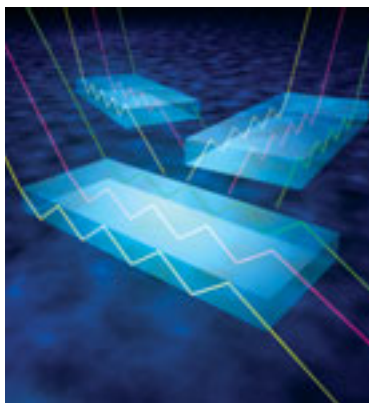
### Future directions

The step-RI single-mode planar waveguide offers some unique ATR measurement capabilities—especially when applied to substrate-supported organic thin films—that are unmatched by other methods. The inherent sensitivity of monochromatic IOW-ATR spectrometry is well known. New developments over the past decade have added multidimensional information to this instrument platform—specifically, broad spectral bandwidth and electrochemical capabilities, which are especially useful to surface and interface scientists.

The multidimensional information offered by broadband ATR spectroelectrochemistry provides a means to potentially discriminate among multiple analytes on the basis of differences in absorbance spectra and reduction potential. This discrimination power can provide selectivity in chemical sensing applications, particularly when the ITO is overcoated with a chemically selective adsorption layer (22).

The most significant practical disadvantage of single-mode IOW spectroscopy is the difficulty of coupling light into the waveguide. Grating and prism coupling require precise alignment to gen-

erate reproducible results; consequently, the types of measurements we have described have thus far been performed primarily in research laboratories. Because of engineering advances accompanying the development of fiber-optics-based telecommunications, coupling light into cylindrical waveguides, including single-mode fibers, is technically much simpler. However, much less power can be coupled into a cylindrical waveguide than into a planar waveguide. In addition, planar geometry offers better control over mode selection and polarization, and it is more compatible with organic and inorganic thin-film deposition technologies, most of which were designed for planar substrates. Current research into hybrid structures, in which fiber coupling is used to direct light into and out of a central, planar section of the waveguide that functions as the spectroscopic platform, may offer an alternative that circumvents the difficulties associated with planar IOW incoupling.



We acknowledge the numerous scientists who made significant contributions to the research described herein, particularly Darren Dunphy, Neal Armstrong, Lin Yang, Lifeng Li, Jim Burke, and John Lee. The National Science Foundation and the National Institutes of Health provided the majority of the funding that supported this research.

*John Thomas Bradshaw is an R&D scientist at Artel. His research focuses on evanescent wave techniques, including waveguide and surface plasmon techniques, and their application to drug discovery problems. Sergio B. Mendes is a research professor and S. Scott Saavedra is a professor at the University of Arizona. Mendes' research interests include biomolecular films, waveguide-based optical spectroscopies, and integrated-optical chemical and biological sensors. Saavedra's research concentrates on biosurface and interface science, chemical and biochemical sensors, and surface spectroscopies. Address correspondence about this article to Saavedra at saavedra@email.arizona.edu.*

## References

- (1) Harrick, N. J. *J. Phys. Chem.* **1960**, *64*, 1110–1114.
- (2) Fahrenfort, J. *Spectrochim. Acta* **1961**, *17*, 698–709.
- (3) Wilks, P. A.; Hirschfeld, T. *Appl. Spectrosc. Rev.* **1967**, *1*, 99–130.
- (4) Harrick, N. J. In *Internal Reflection Spectroscopy*; Harrick Scientific Corp.: Ossining, NY, 1967; pp 13–65.
- (5) Hansen, W. N. *Anal. Chem.* **1963**, *35*, 765–766.
- (6) Tien, P. K. *Appl. Opt.* **1971**, *10*, 2395–2413.
- (7) Plowman, T. E.; Saavedra, S. S.; Reichert, W. M. *Biomaterials* **1998**, *19*, 341–355.
- (8) Lukosz, W. *Sens. Actuators, B* **1995**, *29*, 37–50.
- (9) Bohn, P. W. *Anal. Chem.* **1985**, *57*, 1203–1208.
- (10) Kang, L.; Dessy, R. E. *Crit. Rev. Anal. Chem.* **1990**, *21*, 377–388.
- (11) Bohn, P. W. *Trends Anal. Chem.* **1987**, *6*, 223–233.
- (12) Rabolt, J. F.; Swalen, J. D. In *Advances in Spectroscopy: Spectroscopy of Surfaces*; Hester, R. E., Clark, R. J. H., Eds.; Wiley: Chichester, U.K., 1988; Vol. 16, Chapter 1.
- (13) Kanger, J. S.; et al. *J. Phys. Chem.* **1996**, *100*, 3288–3292.
- (14) Reichert, W. M.; et al. *Appl. Spectrosc.* **1987**, *41*, 636–640.
- (15) Fell, N. F.; Bohn, P. W. *Anal. Chem.* **1993**, *65*, 3382–3388.
- (16) Plowman, T. E.; et al. *Anal. Chem.* **1999**, *71*, 4344–4352.
- (17) Choquette, S. J.; Locascio-Brown, L.; Durst, R. A. *Anal. Chem.* **1992**, *64*, 55–60.
- (18) Rowe, C. A.; et al. *Anal. Chem.* **1999**, *71*, 433–439.
- (19) Saavedra, S. S.; Reichert, W. M. *Langmuir* **1991**, *7*, 995–999.
- (20) Edmiston, P. L.; et al. *J. Am. Chem. Soc.* **1997**, *119*, 560–570.
- (21) Yang, L.; Saavedra, S. S.; Armstrong, N. R. *Anal. Chem.* **1996**, *68*, 1834–1841.
- (22) Ross, S. E.; Seliskar, C. J.; Heineman, W. R. *Anal. Chem.* **2000**, *72*, 5549.
- (23) Puyol, M.; et al. *Anal. Chem.* **1999**, *71*, 5037–5044.
- (24) Degrandpre, M. D.; et al. *Anal. Chem.* **1990**, *62*, 2012–2017.
- (25) Ohno, H.; Fukuda, K.; Kurusu, F. *Chem. Lett.* **2000**, *76*, 77.
- (26) Qi, Z. M.; et al. *Opt. Lett.* **2002**, *27*, 2001–2003.
- (27) Kogelnik, H. In *Topics in Applied Physics: Integrated Optics*, 2nd ed.; Tamir, T., Ed.; Springer-Verlag: Berlin, 1979; Vol. 7, pp 13–81.
- (28) Tamir, T. In *Integrated Optics*; Tamir, T., Ed.; Springer-Verlag: New York, 1975; pp 83–137.
- (29) Mendes, S.; et al. *Appl. Opt.* **1995**, *34*, 6180–6186.
- (30) Mendes, S. B.; Saavedra, S. S. *Appl. Opt.* **2000**, *39*, 612–621.
- (31) Derickson, D. *Fiber Optic Test and Measurement*; Prentice Hall: NJ, 1998.
- (32) Stokes, L. F. *IEEE Circuits and Devices Magazine* **1994**, *10* (1), 46–47.
- (33) Midwinter, J. E. *IEEE J. Quantum Electron.* **1971**, *QE-7*, 345–350.
- (34) Mendes, S. B.; et al. *Langmuir* **1996**, *12*, 3374–3376.
- (35) Mendes, S.; et al. *Opt. Commun.* **1997**, *136*, 320–326.
- (36) Bradshaw, J. T.; Mendes, S. B.; Saavedra, S. S. *Anal. Chem.* **2002**, *74*, 1751–1759.
- (37) Yang, L.; et al. *Anal. Chem.* **1994**, *66*, 1254–1263.
- (38) Kato, K.; et al. *Chem. Lett.* **1995**, 437–438.
- (39) Heineman, W. R.; Hawkridge, F. M.; Blount, H. N. In *Electroanalytical Chemistry*; Bard, A., Ed.; Marcel Dekker: New York, 1984; Vol. 13, pp 1–113.
- (40) Kuwana, T.; Winograd, N. In *Electroanalytical Chemistry*; Bard, A., Ed.; Marcel Dekker: New York, 1974; Vol. 7, pp 1–78.
- (41) Winograd, N.; Kuwana, T. *J. Electroanal. Chem.* **1969**, *23*, 333–342.
- (42) Hansen, W. N.; Kuwana, T.; Osteryoung, R. A. *Anal. Chem.* **1966**, *38*, 1810–1821.
- (43) Hansen, W. N.; Osteryoung, R. A.; Kuwana, T. *J. Am. Chem. Soc.* **1966**, *88*, 1062–1063.
- (44) Itoh, K.; Fujishima, A. In *Electrochemistry in Transition: From the 20th to the 21st Century*; Murphy, O. J., Srinivasan, S., Conway, B. E., Eds.; Plenum: New York, 1992; pp 219–225.
- (45) Itoh, K.; Fujishima, A. *J. Phys. Chem.* **1988**, *92*, 7043–7045.
- (46) Piraud, C.; et al. *Anal. Chem.* **1992**, *64*, 651.
- (47) Dunphy, D. R.; et al. *Anal. Chem.* **1997**, *69*, 3086–3094.
- (48) Dunphy, D. R.; et al.; *Interfacial Electrochemistry*; A. Wieckowski, Ed.; Marcel Dekker: New York, 1999; Chapter 29.
- (49) Matsuda, N.; et al. *Chem. Lett.* **1998**, 125–126.
- (50) Doherty, W. J.; et al. *Appl. Spectrosc.* **2002**, *56*, 920–927.
- (51) Bradshaw, J. T.; et al. *Anal. Chem.* **2003**, *75*, 1080–1088.